Equivalent circuit for VO2 phase change material film in reconfigurable frequency selective surfaces

Varittha Sanphuang, Nima Ghalichechian, Niru K. Nahar, and John L. Volakis

Citation: Applied Physics Letters **107**, 253106 (2015); doi: 10.1063/1.4938468
View online: http://dx.doi.org/10.1063/1.4938468
View Table of Contents: http://scitation.aip.org/content/aip/journal/apl/107/25?ver=pdfcov
Published by the AIP Publishing

Equivalent circuit for VO_2 phase change material film in reconfigurable frequency selective surfaces

Varittha Sanphuang, Nima Ghalichechian, Niru K. Nahar, and John L. Volakis
Department of Electrical and Computer Engineering, ElectroScience Laboratory, The Ohio State University, Columbus, Ohio 43212, USA

(Received 18 August 2015; accepted 10 December 2015; published online 24 December 2015)

We developed equivalent circuits of phase change materials based on vanadium dioxide (VO_2) thin films. These circuits are used to model VO_2 thin films for reconfigurable frequency selective surfaces (FSSs). This is important as it provides a way for designing complex structures. A reconfigurable FSS filter using VO_2 ON/OFF switches is designed demonstrating −60 dB isolation between the states. This filter is used to provide the transmission and reflection responses of the FSS in the frequency range of 0.1–0.6 THz. The comparison between equivalent circuit and full-wave simulation shows excellent agreement. © *2015 AIP Publishing LLC*.
[http://dx.doi.org/10.1063/1.4938468]

Reconfigurability is important in RF, millimeter wave, and terahertz and optical systems for sensing, imaging, wireless, and satellite communications. Indeed, significant efforts have been devoted in the past to develop tunable systems using PIN[1,2] and Schottky diodes,[2] varactors,[2] FET,[3] and RF MEMS switches.[2,4–6] RF MEMS switches are attractive at high frequency due to their low power consumption, low insertion loss, and high linearity.[7] However, RF MEMS switches often suffer from reliability and high voltage actuation issues. Phase change materials (PCMs) are an alternative to RF MEMS switches and have the potential to overcome the aforementioned issues.

PCMs belong to a class of materials whose conductivity and permittivity change drastically with temperature. Various PCM materials have been researched[8–11] corresponding to a wide range of transition temperatures. However, more than half of them[11] have their transition temperature from dielectric phase to conductor phase way below room temperature, implying that a cooling system is needed for triggering the switch. Understandably, for all practical purposes, we require PCMs where a heater is employed. Among various PCMs, the one based on vanadium dioxide (VO_2) has a phase transition closest to room temperature. This temperature is around 68 °C (∼340 K) and is associated with large conductivity change of the VO_2 PCM on the order of $\sim 10^4$. Combined with the fabrication ease of VO_2 films, this PCM is more attractive. Specifically, VO_2 films can be deposited using standard microfabrication techniques and patterned via lithographic processes. Therefore, they can be fabricated at low cost using batch processes. Furthermore, the reversible change between dielectric and conductor of VO_2 films makes them attractive for reconfiguration. Several applications with reconfiguration were proposed in the past,[12–20] for example, thermal switches, thermal sensor, reconfigurable optical devices, and ON/OFF THz spatial filter with integrated micro-heater.[20] The micro-heater is introduced around the filter to easily control the temperature for practical realization as shown in Fig. 1. However, none of previous reconfigurable studies used an equivalent circuit to study for the VO_2 thin film. Using such an equivalent circuit, we can carry out full-wave analysis and design for further understanding of the VO_2 film characteristics before and during fabrication.

In this paper, the equivalent circuits of VO_2 thin film are developed and used to reconfigure frequency selective surface (FSS) as the film changes its states between dielectric and conductor phases. In the following sections, we discuss the VO_2 thin film fabrication and provide resistivity measurements to obtain the conductivity values for the circuit design. For analysis, we employ the equivalent circuit of the VO_2 at both phases. The VO_2 film is then introduced into the FSS structures and its reconfigurable responses are obtained.

The VO_2 film was grown using a DC reactive magnetron sputtering process. This provides for a conformal and uniform film growth with a relatively low-cost batch process. Specifically, the AJA Orion DC sputtering system was employed with a 99.5% vanadium (V) target on a 2″ *c*-plane (0001) sapphire substrate. Oxygen was then injected as a reactive gas to create the oxide from the V target. Several attempts were made to optimize the growth conditions, i.e., O_2/Ar flow ratio (7.5%) and deposition temperature (650 °C).

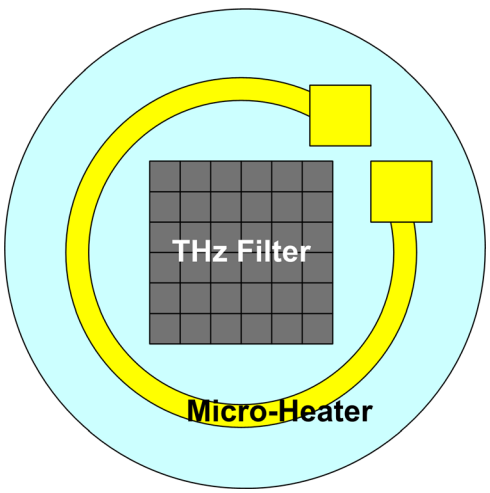

FIG. 1. An example of circular loop micro-heater to control the temperature of VO_2 film around the THz filter.

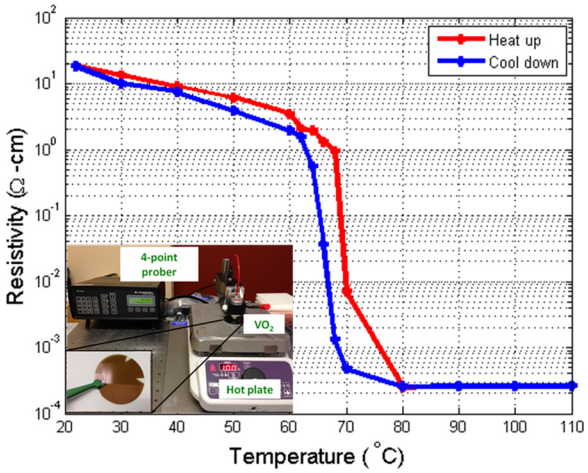

FIG. 2. Resistivity vs temperature hysteresis of the VO_2 sample. (Inset: resistivity measurement setup with an example of VO_2 thin film deposited on Al_2O_3 substrate).

To observe the phase change property of the grown VO_2 film, its resistivity and temperature hysteresis loop were measured. It was found that the maximum resistivity ratio between the heated and cooled states was 7×10^4. The transition is observed to occur at 68 °C and the relevant curve is shown in Fig. 2. It is important to note that the film exhibits small hysteresis. The measurement setup is used to obtain the curve as shown in the inset of Fig. 1. As depicted, a four-point probe (Jandel RM3000) was used to accurately extract the film's sheet resistance. A hot plate was also positioned under the four-point probe to control and vary the temperature of the film in 2–10 °C steps. The measured conductivity (σ) of our thin film at two different temperatures represents its dielectric ($\sigma = 5.38$ S/m) and conductor phases ($\sigma = 3.77 \times 10^5$ S/m), respectively.[19] Two equivalent circuits were modeled for the VO_2 film corresponding to its two states using the fabricated film conductivity values. These are discussed below.

In its dielectric phase ($\sigma = 5.38$ S/m from measurement), the VO_2 film can be modeled as a transmission line represented by a shunt capacitor and a resistor as shown in Fig. 3. The capacitance is obtained by

$$C = \frac{\varepsilon_0 \varepsilon_r A}{t}, \tag{1}$$

where C is the film's capacitance, ε_0 is permittivity of free-space, ε_r is the dielectric constant of VO_2 ($\varepsilon_r = 36$ in dielectric phase[21–24]), A is the surface area of the film (150 μm $\times$ 150 μm as used in our design), and t is the film thickness (65 nm) with these parameters, $C = 106.5$ pF. Also the resistance R is added referring to the losses in the dielectric itself. The value of $R = 0.41 \times 10^6\ \Omega$ was optimized to map the simulation result accordingly. Again, note that the full-wave simulation results are modeled based on the measured conductivities of both states throughout this study to ensure the accuracy of the proposed circuit models.

Next, we proceeded to compare the circuit's response using Advanced Design System (ADS) to the full-wave simulation (Ansoft HFSS) across the frequency range of 0.1–1 THz. As seen in Fig. 3, the agreement is excellent. We note that at the dielectric phase of the VO_2, the entire signal is perfectly transmitted.

As the temperature increases and the VO_2 film changes to its conductor phase ($\sigma = 3.77 \times 10^5$ S/m from measurement), its transmission and reflection properties can be modeled using a shunt inductance (L) and a series resistance (R). This is depicted in Fig. 4 along with the response of the equivalent circuit, showing good agreement from 0.1 to 1 THz. We observe that at the conductor phase, the reflection is almost 100%, implying that the VO_2 behaves as a conductor. The optimization based on simulation results led to a circuit having L = 15 fH and R = 100 Ω.

To demonstrate an application using the VO_2 equivalent circuit, the VO_2 film was fabricated as part of the FSS to perform a bandpass or a bandstop filter.[25,26] Using the VO_2 properties, the FSS presence can be turned on and off as needed and by doing so the FSS changes from bandstop to bandpass. As usual, the element type (geometry), substrate, superstrate, and inter-element spacing play a significant role in the performance of the FSS.[26]

The proposed THz FSS filter unit cell is depicted in Fig. 5. Each cell is designed using a cross loop slot FSS

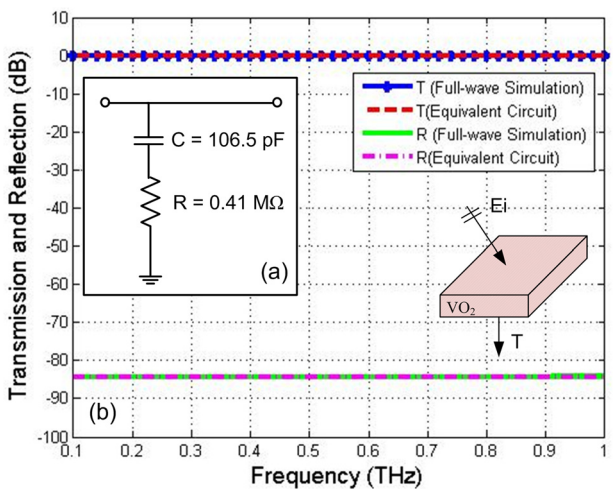

FIG. 3. The comparison of the transmission (T) and reflection (R) responses between full-wave simulation and the equivalent circuit. The actual equivalent circuit of the dielectric phase is shown at the inset.

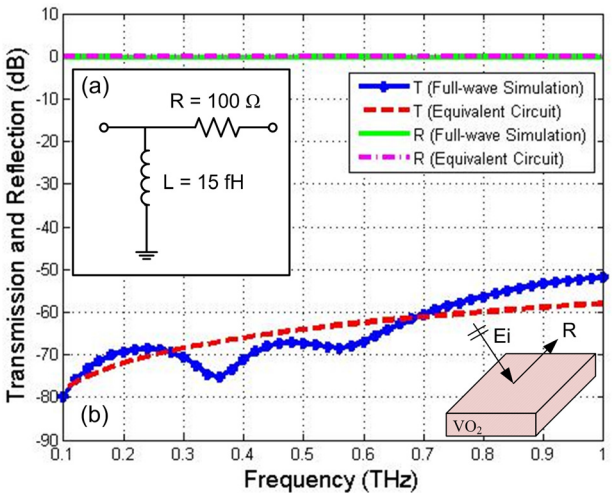

FIG. 4. The comparison of transmission (T) and reflection (R) responses between full-wave simulation and the equivalent circuit. The actual equivalent circuit of the conductor phase is shown at the inset.

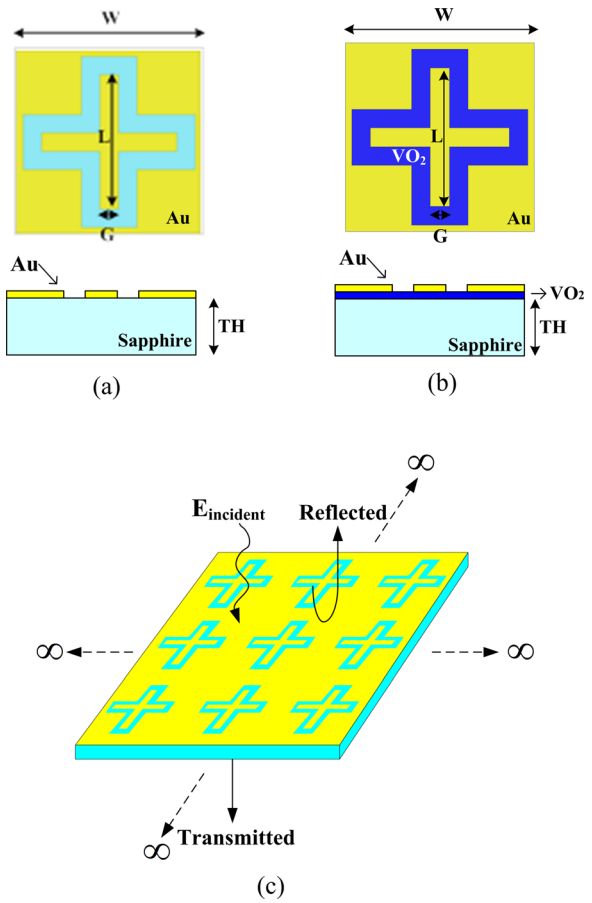

FIG. 5. Cross loop slot FSS unit cell: top view and side view (a) FSS slot without VO_2 thin film, (b) with VO_2 thin film, (c) overall structure.

fabricated using a gold layer on top of a c-plane sapphire substrate having a dielectric constant $\varepsilon_r = 10$. The cross loop structure was chosen as it provides additional degree of freedom for the filter. The sapphire substrate is preferable at THz frequency because of its high transparency at this band. For the cross loop slot FSS, the design parameters are as follows: (1) unit cell dimension, $W = 150\,\mu m$; (2) cross leg length, $L = 110\,\mu m$; (3) cross leg width, $G = 15\,\mu m$; (4) substrate thickness, $TH = 50\,\mu m$; and (5) metal thickness, $t = 150\,nm$.

In our design, the slot of the cross loop FSS is backed by the VO_2 thin film placed between FSS metal and substrate. The ON/OFF states of the VO_2 thin film will then be used to turn on and off the FSS filter function.

The equivalent circuit model of the proposed cross loop FSS in Fig. 5 is provided in Fig. 6(a) in the absence of VO_2 thin film. As depicted, Port 1 represents the incident wave and Port 2 is the location where the transmitted wave is observed. The dielectric substrate is modeled as a transmission line having an impedance of Z_1 as wave impedance in dielectric calculated by[27]

$$Z_1 = \sqrt{\frac{\mu}{\varepsilon}} = \sqrt{\frac{\mu_0}{\varepsilon_0 \varepsilon_r}} = 119.22\ \Omega, \tag{2}$$

where μ_0, permeability of free-space is $4\pi \times 10^{-7}$ H/m, ε_0, permittivity of free-space is 8.854×10^{-12} F/m, and ε_r, the dielectric constant of substrate, which in this case is 10 for sapphire. Then the length of transmission line, l, equals to the thickness of the substrate in electrical length (θ) as

$$\theta = \frac{2\pi}{\lambda\sqrt{\varepsilon_r}} TH = 5.69^\circ, \tag{3}$$

where λ, the wavelength is 1 mm at frequency of 0.3 THz and TH, the substrate thickness is 50 μm.

Next, the FSS is modeled as a parallel RLC with the resistor placed next to capacitor as depicted in Fig. 6(a). The RLC values are $R_1 = 1\,\Omega$, $C_1 = 59.36\,fF$, and $L_1 = 4.31\,pH$ and its accuracy was validated via full-wave simulation. For the transmission curves in Fig. 6(b), we observe good agreement between the circuit model and the corresponding full-wave simulations with a small deviation at the higher band.

Thin film VO_2 (65 nm thick) is usually deposited in between substrate and metal as depicted in the inset of Fig. 6(c). This process is intended to create the slot that has VO_2 thin film underneath FSS metal with the same structure as in Fig. 4. The circuit model of the FSS with the inserted FSS VO_2 is given in Figs. 6(c) and 6(d). The simulated curves in Fig. 6 refer to the conditions: below and above 68 °C. These correspond to the dielectric and conductor phases of the VO_2 thin film and showed good agreement with full-wave simulations. We also observe that below ~68 °C, the filter shows a transmission peak at 0.3 THz. Of most importance is that the contrast between transmission and reflection at 0.3 THz is greater than 60 dB. As seen, the filter is off when the temperature increases ≳68 °C (total reflection). We also observe that the out of band loss is only −2 dB.

Even though the proposed filter geometry here has not been fabricated, one of our previous works on this topic provides an example of a real device as ON/OFF THz filter with the measurement validation that supports the physics of this study. The measurement results present the verification of VO_2 PCM films integrated in the THz filter for switching, achieving ON/OFF switch as the conductivity of VO_2 film changes when the filter is heated as shown in Fig. 7.[25]

Standard photolithography, thin film deposition, and lift-off techniques were used for fabricating the circular shape ON/OFF filter. First, the VO_2 thin film was deposited using DC sputtering. Next the photolithography steps with image-reversal AZ5214E photoresist were used to pattern the periodic structure and micro-heater. Then, a gold layer was deposited using e-beam evaporator (CHA Solution) followed by a lift-off step to achieve the final structures. Finally, the transmissions of the fabricated THz filter for both states were measured using a time domain spectroscopy (TPS 3000 system, TeraView Ltd.) at normal incidence.

We presented equivalent circuits for the VO_2 thin film when this film is at dielectric and conductor phases. These equivalent circuits were used to design and evaluate a traditional cross slot FSS. Specifically, the VO_2 thin film was used to turn ON and OFF the slot of the FSS. In this case, ON refers to the conductor phase and OFF refers to the dielectric phase of the VO_2 film. The obtained circuit analysis results for the transmission and reflection of the band-pass/bandstop FSS demonstrated quite accurate and are in good agreement with the full-wave simulations. This

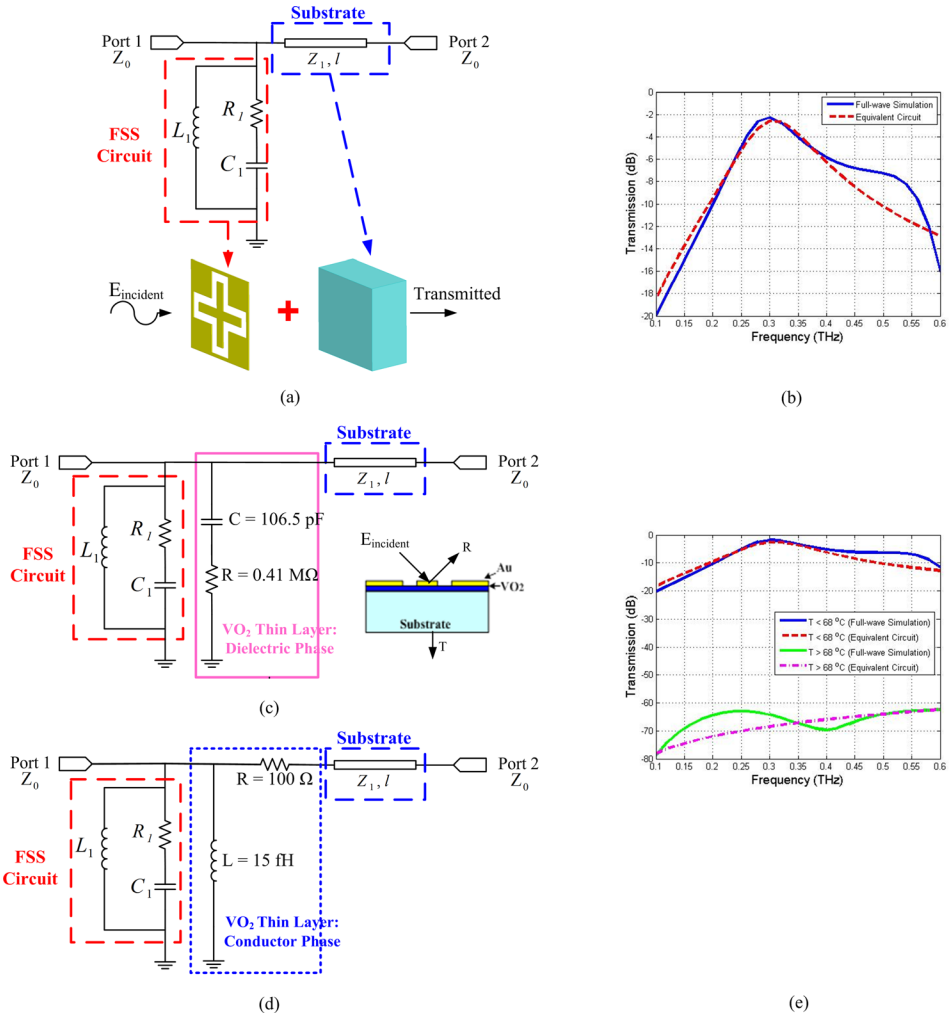

FIG. 6. (a) Equivalent circuit of proposed FSS filter. (b) Comparison between equivalent circuit and full-wave simulation. (c) Equivalent circuit of the cross slot FSS filter with VO_2 placed between FSS metal and substrate at dielectric phase. (d) Equivalent circuit of the cross slot FSS filter with VO_2 placed between FSS metal and substrate at conductor phase. (e) Comparison of transmission (T) and reflection (R) coefficient using the equivalent circuits and full-wave simulations.

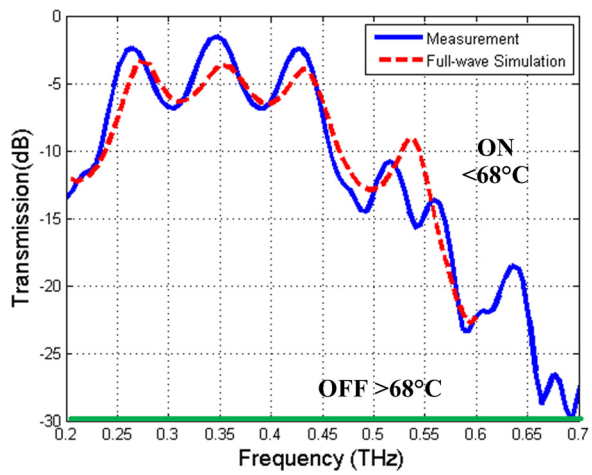

FIG. 7. Comparison of simulated vs measured transmission responses for THz FSS filter at below and above 68 °C.

equivalent circuit improves the understanding of the reconfigurable systems when the VO_2 film is integrated into the structure and provides a way to design and optimize complex structures before fabrication.

[1]S. Nikolaou, R. Bairavasubramanian, C. Lugo, I. Carrasquillo, D. C. Thompson, G. E. Ponchak, J. Papapolymerou, and M. M. Tentzeris, IEEE Antennas Propag. Mag. **54**(2), 439 (2006).
[2]C. G. Christodoulou, Y. Tawk, S. A. Lane, and S. R. Erwin, Proc. IEEE **100**(7), 2250 (2012).
[3]T. Aboufoul, A. Alomainy, and C. Parini, IEEE Antennas Wireless Propag. Lett. **11**, 392 (2012).
[4]G. M. Rebeiz, K. Entesari, I. Reines, S. Park, M. A. El-Tanani, A. Grichener, and A. R. Brown, IEEE Microwave Mag. **10**, 55 (2009).
[5]T. Hirano, K. Miyazaki, M. Hatamoto, R. Yasumitsu, K. Hama, and F. Watanabe, in *Proceedings of the Second European Conference on Antennas and Propagation (EuCAP)*, Edinburgh, Scotland, 11–16 November 2007, pp. 1–5.
[6]N. Haridas, A. T. Erdogan, T. Arslan, A. J. Walton, S. Smith, T. Stevenson, C. Dunare, A. Gundlach, J. Terry, P. Argyrakis, K. Tierney, A. Ross, and T. O'Hara, in *Proceedings of the NASA/ESA Conference on Adaptive Hardware and Systems, AHS*, Noordwijk, Netherlands, 22–25 June 2008, pp. 147–154.
[7]G. M. Rebeiz, *RF MEMS Theory, Design and Technology* (Wiley, New Jersey, 2003).
[8]N. F. Mott, *Metal-Insulator Transitions* (Taylor & Francis, London, 1990), p. 286.
[9]M. Imada, A. Fujimori, and Y. Tokura, Rev. Mod. Phys. **70**, 1039 (1998).
[10]A. Adler, Rev. Mod. Phys. **40**, 714 (1968).
[11]Z. Yang, C. Ko, and S. Ramanathan, Annu. Rev. Mater. Res. **41**, 337 (2011).
[12]G. Stefanovich, A. Pergament, and D. Stefanovich, J. Phys.: Condens. Matter **12**, 8837 (2000).
[13]P. P. Boriskov, A. A. Velichko, A. L. Pergament, G. B. Stefanovich, and D. G. Stefanovich, Tech. Phys. Lett. **28**, 406 (2002).
[14]B.-J. Kim, Y. W. Lee, B.-G. Chae, S. J. Yun, S.-Y. Oh, H.-T. Kim, and Y.-S. Lim, Appl. Phys. Lett. **90**, 023515 (2007).
[15]H. N. S. Krishnamoorthy, Y. Zhou, S. Ramanathan, E. Narimanov, and V. M. Menon, Appl. Phys. Lett. **104**, 121101 (2014).
[16]H. T. Chen, W. J. Padilla, J. M. O. Zide, A. C. Gossard, A. J. Taylor, and R. D. Averitt, Nature **444**, 597 (2006).

[17]A. Crunteanu, J. Leroy, G. Humbert, D. Ferachou, J.-C. Orlianges, C. Champeaux, and P. Blondy, in *Proceedings of the IEEE MTT-S International Microwave Symposium Digest, MTT*, Montreal, QC, Canada, 17–22 June 2012, pp. 1–3.
[18]V. Sanphuang, N. Ghalichechian, N. K. Nahar, and J. L. Volakis, in *Proceedings of the USNC-URSI Radio Science Meeting*, Memphis, TN, USA, 6–11 July 2014, p. 209.
[19]V. Sanphuang, N. Ghalichechian, N. K. Nahar, and J. L. Volakis, in Proceedings of the IEEE Antennas and Propagation Society International Symposium, APS/URSI, Vancouver, BC, Canada, 19–25 July 2015.
[20]V. Sanphuang, N. Ghalichechian, N. K. Nahar, and J. L. Volakis, in *Proceedings of the IEEE Antennas and Propagation Society International Symposium, APS/URSI*, Memphis, TN, USA, 6–11 July 2014, pp. 565–566.
[21]Z. Yang, C. Ko, V. Balakrishnan, G. Gopalakrishnan, and S. Ramanatha, Phys. Rev. B **82**, 205101 (2010).
[22]P. J. Hood and J. F. Denatale, J. Appl. Phys. **70**(1), 376–381 (1991).
[23]A. Zylbersztejn, B. Pannetier, and P. Merenda, Phys. Rev. Lett. B **11**, 4383 (1975).
[24]A. B. Barker, H. W. Verleur, and H. J. Guggenheim, Phys. Rev. Lett. **17**, 1286 (1966).
[25]V. Sanphuang, N. Ghalichechian, N. K. Nahar, and J. L. Volakis, in *Proceedings of the IEEE National Aerospace and Electronics Conference, NAECON*, Dayton, OH, USA, 24–27 June 2014, pp. 319–320.
[26]B. A. Munk, *Frequency Selective Surfaces, Theory and Design* (Wiley-Interscience, New York, 2000).
[27]D. M. Pozar, *Microwave Engineering* (John Wiley & sons, Inc, New Jersey, 2005).